Polarization spectroscopy of an excited state transition

Christopher Carr, Charles S. Adams, and Kevin J. Weatherill*

Department of Physics, Durham University, South Road, Durham, DH1 3LE, UK

**Corresponding author: k.j.weatherill@durham.ac.uk*

Received July 19, 2011; revised October 20, 2011; accepted November 17, 2011;
posted November 17, 2011 (Doc. ID 151067); published January 18, 2012

We demonstrate polarization spectroscopy of an excited state transition in room-temperature cesium vapor. An anisotropy induced by a circularly polarized pump beam on the D2 transition is observed using a weak probe on the $6P_{3/2} \rightarrow 7S_{1/2}$ transition. At high pump power, a subfeature due to Autler-Townes splitting is observed that theoretical modeling shows is enhanced by Doppler averaging. Polarization spectroscopy provides a simple modulation–free signal suitable for laser frequency stabilization to excited state transitions. © 2012 Optical Society of America

OCIS codes: 020.1670, 020.3690, 140.3425, 300.6210.

Polarization spectroscopy [1] is a widely used Doppler-free technique that can provide a robust and modulation-free signal to which a laser can be frequency stabilized [2]. The technique has predominantly been used on strong optical transitions from the ground state of atomic vapors [3] where optical pumping induces birefringence in the medium or where birefringence is due to saturation effects [4]. In addition to ground state transitions, excited state spectroscopy is of growing interest for applications such as the search for stable frequency references [5], Rydberg gases [6] and their application to electro-optics [7] and nonlinear optics [8], state lifetime measurement [9], optical filtering [10], multiphoton laser cooling [11], frequency up-conversion [12] and frequency stabilization [13]. In this work we extend the use of polarization spectroscopy to excited state transitions. By probing an infrared excited state transition with a large dipole moment we observe significant absorption and spectra with a signal to noise ratio of more than 2×10^3.

A schematic of the experimental setup is shown in Fig. 1(a). A circularly polarized 852 nm pump beam stabilized to the $6S_{1/2}$, $F = 4 \rightarrow 6P_{3/2}$, $F' = 5$ transition, passes through a Cs room-temperature vapor cell. A counterpropagating linearly polarized 1470 nm probe beam is scanned across the $6P_{3/2}$ $F' = 5 \rightarrow 7S_{1/2}$, $F'' = 4$ transition. The scan is calibrated using a wavemeter to better than 1% precision. The relevant atomic level structure is shown in Fig. 1(b). The pump drives σ^+ transitions and transfers population toward the $|F', m_F = F'\rangle$ state, inducing an anisotropy in the medium. On the excited state transition, the component of the probe that drives σ^- transitions is preferentially absorbed because there are no σ^+ allowed transitions from the $|F', m_F = F'\rangle$ state, resulting in a change in polarization of the probe. The electric field of the probe after the cell is $\vec{E} = \vec{E}_+ + \vec{E}_-$, [14] where

$$\vec{E}_\pm = E_0 \exp\left(\frac{i\omega n_\pm L}{c} - \frac{\alpha_\pm L}{2}\right) \frac{\exp(\mp i\phi)}{2} (\hat{x} \pm i\hat{y}). \quad (1)$$

The refractive indices $n_\pm$ and absorption coefficients $\alpha_\pm$ of the vapor are for circular polarization driving $\sigma^\pm$ transitions. We also define $\Delta n = n^+ - n^-$ and $\Delta\alpha = \alpha^+ - \alpha^-$.

A polarizing beam splitter cube oriented at angle $\phi = 45°$ to the polarization vector of the probe resolves the probe electric field into orthogonal linear components that are detected using two Ge photodiodes. The resolved components S_1 and S_2 are proportional to $|\vec{E}|^2$ and are normalized so that the off-resonance transmission is 1. Thus, $(S_1 + S_2)/2 \propto \Delta\alpha$ and the anisotropy $(S_1 - S_2)/2 \propto \Delta n$. Figure 2 shows spectra obtained for a pump power of 500 μW and probe power of 10 μW. Figure 2(a) shows the individual spectra S_1 and S_2 recorded at the two photodiodes as a function of probe detuning while Fig. 2(b) shows $(S_1 + S_2)/2$, which is a Lorentzian profile with FWHM Γ that can be written as

$$\Delta\alpha = \frac{\Delta\alpha_0}{1 + (2\Delta_{\text{probe}}/\Gamma)^2}, \quad (2)$$

where Δ_{probe} is the detuning of the probe laser from resonance and $\Delta\alpha_0$ is the maximum difference in absorption at the line center. Figure 2(c) shows the polarization spectrum $(S_1 - S_2)/2$. This signal is proportional to the dispersion described by

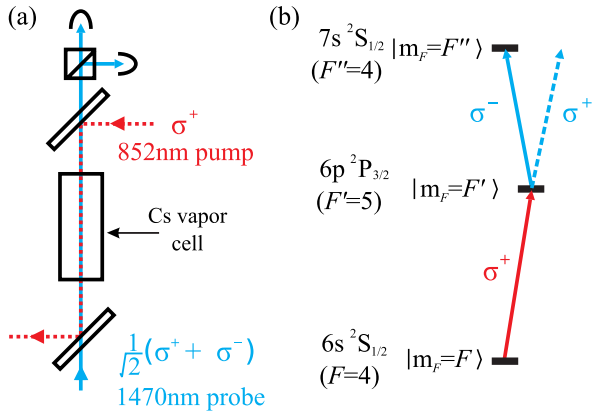

Fig. 1. (Color online) (a) Experimental setup. The 852 nm pump (1.6 mm $1/e^2$ radius) and 1470 nm probe (1.2 mm $1/e^2$ radius) beams counterpropagate through a 5 cm vapor cell. Probe rotation is measured by a polarimeter. (b) Energy level diagram. The circularly polarized pump with Rabi frequency Ω_{pump} drives σ^+ transitions and induces an anisotropy in the medium. The medium is probed by a linearly polarized beam with Rabi frequency Ω_{probe} on the excited state transition. The excited state linewidths $\Gamma_{6P} = 5.2$ MHz and $\Gamma_{7S} = 3.3$ MHz [15].

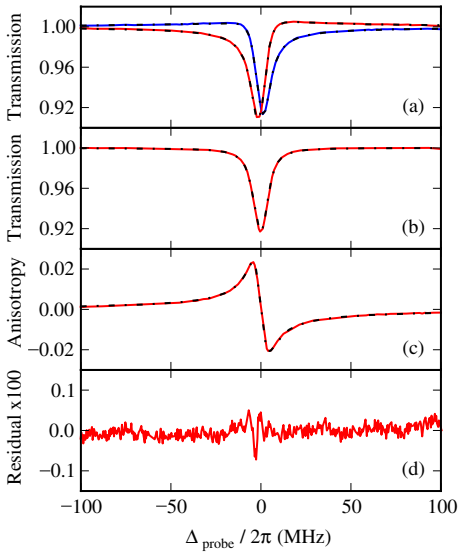

Fig. 2. (Color online) Experimental spectra with theoretical fitting (dashed lines). (a) Individual signals S_1 (red line) and S_2 (blue line) recorded at the two photodiodes. (b) $(S_1 + S_2)/2$ is a Lorentzian absorption profile and (c) $(S_1 - S_2)/2$ is a dispersive shaped profile for the excited state transition. (d) The residual of the fit to the data shown in (c).

$$\Delta n = \Delta\alpha_0 \frac{2c}{\omega_0 \Gamma} \frac{\Delta_{\text{probe}}}{1 + (2\Delta_{\text{probe}}/\Gamma)^2}. \tag{3}$$

S_1 and S_2 are fit using a combination of Eqs. (2) and (3), yielding the linewidth Γ of the main feature. Figure 2(d) shows the residual to the fit of the data in Fig. 2(c); the largest discrepancy (less than 0.1%) arises from short-term fluctuations of the probe frequency at the two-photon resonance.

Figure 3 shows the development of the polarization spectrum as a function of pump power. As the pump intensity is increased, the magnitude of the feature increases until the pump transition is saturated. The linewidth also increases with power broadening and eventually displays an Autler-Townes splitting (ATS) [16]. As the ATS becomes resolved, a subfeature at the center of the main lineshape appears that has the opposite gradient to the main signal. In this regime it is no longer possible to model the data using a single Lorentzian and its concomitant dispersion; however, an excellent fit is obtained using a pair of displaced absorption/dispersion lineshapes of the same width. We can

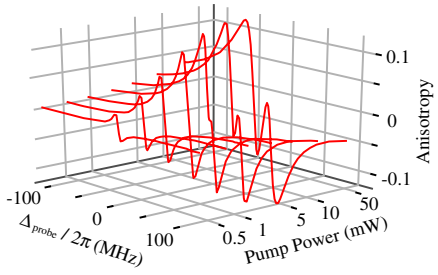

Fig. 3. (Color online) Experimental data. Evolution of the polarization spectra with increasing pump power.

therefore objectively distinguish our ATS system from electromagnetically induced transparency [17].

The evolution of the on-resonance gradient and width of the features with pump power are shown in Fig. 4(a) and 4(b), respectively. The on-resonance gradient decreases with pump power before increasing and changing sign with the appearance of the subfeature at approximately 4.1 mW. Figure 4(b) shows the width of the main and subfeatures. In both cases, the width is defined as the peak-to-peak frequency difference.

In the weak pump limit $\Omega_{\text{pump}} \ll \Gamma_{6P}$, the minimum linewidth for an atom at rest is Γ_{7S} due to coherent driving of the two-photon transition. With Doppler broadening, we observe a minimum linewidth of the main feature consistent with $\Gamma_{7S} + \Gamma_{6P}(k_{\text{pump}} - k_{\text{probe}})/k_{\text{pump}}$, which can be derived analytically from the optical Bloch equations for a weak probe. The measured width of the subfeature can be less than Γ_{7S}; however this is still consistent with the ATS picture of two displaced Lorentzians. Note also that the slope of the subfeature is always smaller than the maximum slope of the main feature. The width of the features increases with the square root of the pump power as expected.

To investigate the role of Doppler averaging on the dispersive subfeature we solve the optical Bloch equations for the temporal evolution of the system including the component of the thermal velocity of the room-temperature atoms in the direction of the beams. The density matrix approach provides a simplified description of the three-level system with diagonal elements ρ_{11}, ρ_{22}, and ρ_{33} being the populations of the $6S_{1/2}$, $6P_{3/2}$, and $7S_{1/2}$ states, respectively. The off-diagonal elements are the coherences between the states where the decay rates of the $7S_{1/2}$ and $6P_{3/2}$ states are 48.2 ns and 29.5 ns, respectively [15]. We consider the real part of the coherence between the intermediate and excited state $\text{Re}(\rho_{23})$ as it is proportional to the probe dispersion and thus our experimental spectra.

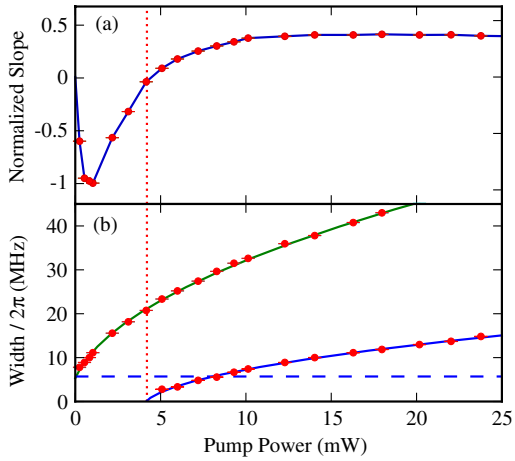

Fig. 4. (Color online) Analysis of dispersive lineshapes. (a) Measured gradient of the signal at $\Delta_{\text{probe}} = 0$ for varying pump power normalized to the maximum gradient. The solid line is a guide to the eye. The dotted vertical line indicates zero gradient. (b) Measured width of the main feature and subfeature with $\sqrt{P}$ scaling (solid lines). The dashed line indicates the Doppler-broadened natural linewidth of the excited state transition.

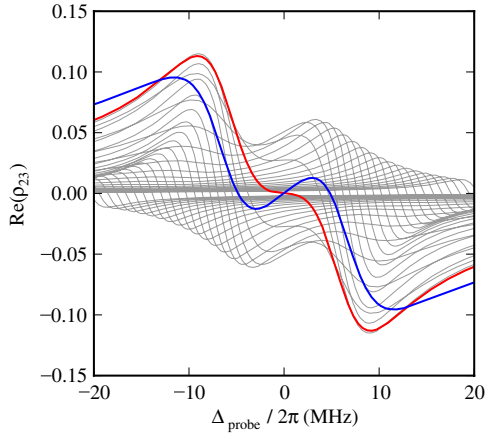

Fig. 5. (Color online) Theoretical modeling of lineshapes. The red line is the lineshape for zero velocity atoms. The blue line is the Doppler-averaged lineshape, multiplied by a factor of 4, for room-temperature atoms. Each gray line represents a velocity class separated by 2 m/s.

Figure 5 shows the solution of the optical Bloch equations for $\mathrm{Re}(\rho_{23})$ using $\Omega_{\mathrm{pump}}/2\pi = 12.2$ MHz and $\Omega_{\mathrm{probe}}/2\pi = 3.3$ MHz to match the average Rabi frequencies experienced by the atoms across the cell in the experiment. This simple model shows good qualitative agreement with the data but quantitative agreement requires integration over the intensity profile of the beams as they are absorbed across the cell. An atom at rest has a dispersive feature with a negative gradient on-resonance (red line). However, when nonzero velocity contributions are included (gray lines), the subfeature is enhanced (blue line). Similar narrowing effects of thermal averaging have been observed in other systems [18,19].

The dispersive shaped feature from excited state polarization spectroscopy provides a convenient discriminant for laser frequency stabilization. In future work we will apply this technique to the intermediate step of a three-photon excitation scheme [20] for use in Rydberg atom experiments [8] and in the creation of ultracold ion and electron beams from laser-cooled atoms [21,22].

We thank I. Hughes, R. Potvliege, and M. Tanasittikosol for discussions and acknowledge support from Durham University and the UK Engineering and Physical Sciences Research Council.

References

1. C. Wieman and T. W. Hänsch, Phys. Rev. Lett. **36**, 1170 (1976).
2. C. P. Pearman, C. S. Adams, S. G. Cox, P. F. Griffin, D. A. Smith, and I. G. Hughes, J. Phys. B **35**, 5141 (2002).
3. M. L. Harris, C. S. Adams, S. L. Cornish, I. C. McLeod, E. Tarleton, and I. G. Hughes, Phys. Rev. A **73**, 062509 (2006).
4. C. Javaux, I. G. Hughes, G. Lochead, J. Millen, and M. P. A. Jones, Eur. Phys. J. D **57**, 151 (2010).
5. M. Breton, N. Cyr, P. Tremblay, M. Têtu, and R. Boucher, IEEE Trans. Instrum. Meas. **42**, 162 (1993).
6. I. Mourachko, D. Comparat, F. de Tomasi, A. Fioretti, P. Nosbaum, V. M. Akulin, and P. Pillet, Phys. Rev. Lett. **80**, 253 (1998).
7. A. K. Mohapatra, M. G. Bason, B. Butscher, K. J. Weatherill, and C. S. Adams, Nat. Phys. **4**, 890 (2008).
8. J. D. Pritchard, D. Maxwell, A. Gauguet, K. J. Weatherill, M. P. A. Jones, and C. S. Adams, Phys. Rev. Lett. **105**, 193603 (2010).
9. D. Sheng, A. Pérez Galván, and L. A. Orozco, Phys. Rev. A **78** 062506 (2008).
10. R. I. Billmers, S. K. Gayen, M. F. Squicciarini, V. M. Contarino, and W. J. Scharpf, Opt. Lett. **20**, 106 (1995).
11. S. Wu, T. Plisson, R. C. Brown, W. D. Phillips, and J. V. Porto, Phys. Rev. Lett. **103**, 173003 (2009).
12. T. Meijer, J. D. White, B. Smeets, M. Jeppesen, and R. E. Scholten, Opt. Lett. **31**, 1002 (2006).
13. R. P. Abel, A. K. Mohapatra, M. G. Bason, J. D. Pritchard, K. J. Weatherill, U. Raitzsch, and C. S. Adams, Appl. Phys. Lett. **94**, 071107 (2009).
14. I. G. Hughes, *New Trends in Quantum Coherence and Nonlinear Optics* (Nova, 2009).
15. C. E. Theodosiou, Phys. Rev. A **30**, 2881 (1984).
16. M. Fleischhauer, A. Imamoglu, and J. P. Marangos, Rev. Mod. Phys. **77**, 633 (2005).
17. P. M. Anisimov, J. P. Dowling, and B. C. Sanders, Phys. Rev. Lett. **107**, 163604 (2011).
18. C. Y. Ye, A. S. Zibrov, Yu. V. Rostovtsev, and M. O. Scully, Phys. Rev. A **65**, 043805 (2002).
19. M. G. Bason, A. K. Mohapatra, K. J. Weatherill, and C. S. Adams, J. Phys. B **42**, 075503 (2009).
20. T. Vogt, M. Viteau, J. Zhao, A. Chotia, D. Comparat, and P. Pillet, Phys. Rev. Lett. **97**, 083003 (2006).
21. B. J. Claessens, S. B. van der Geer, G. Taban, E. J. D. Vredenbregt, and O. J. Luiten, Phys. Rev. Lett. **95**, 164801 (2005).
22. J. L. Hanssen, J. J. McClelland, E. A. Dakin, and M. Jacka, Phys. Rev. A **74**, 063416 (2006).